IOSR Journal of Mechanical and Civil Engineering (IOSR-JMCE)
e-ISSN: 2278-1684, p-ISSN: 2320-334X
PP 54-62
www.iosrjournals.org

Pressure Distribution Around Net Clad Scaffolds Using Computation Fluid Dynamics Techniques

Hassan Irtaza[1], R.G. Beale[2], M.H.R. Godley[2], A. Jameel[3]
[1](Department of Civil Engineering, A.M.U., Aligarh 202002, India)
[2]([2]Faculty of Technology, Design and Environment, Oxford Brookes University, Oxford, U.K.)
[3](University Polytechnic, A.M.U., Aligarh 202002, India)

ABSTRACT : *Computational Fluid Dynamics simulations of the flow patterns and pressure distributions around scaffolds clad by debris netting were undertaken using Fluent. The models were verified using full-scale data from the Silsoe experimental site and from wind tunnel investigations of the permeability of scaffold nets and from fully clad scaffold models. The simulations show that for net clad scaffolds the Eurocode provisions are correct for the pressure coefficients on windward and side faces. However, for leeward faces a net scaffold a pressure coefficient of zero can be used*.

Keywords - *Scaffold structures, Wind loads, Computational fluid dynamics, Pressure coefficients*

1. Introduction

Steel scaffolds are extensively used to provide access and support to permanent works during different stages of construction in the UK and other parts of the world. Previous researches into scaffold structures, both experimentally and computationally, have primarily been involved with determining the structural performance. This includes analyses based on effective length in the early stages of research to more advanced non-linear force displacement effects (local as well as global) taking into account the influence of semi-rigid connections and including both material and geometric non-linearity (Beale, 2007) [1]. Limited research has been reported on the magnitude of loads actually acting on the scaffold including wind load.

Scaffolds are often clad with nets called debris nets as shown in Fig. 1 to protect both the passers-by and work force from falling debris and also to shield workers from extreme weather. Debris nets are generally woven fabric of varying air penetrability. The main disadvantage of using nets is that there is an increase in the wind load on the structure, particularly on the scaffold to building ties. Such increases in the wind load on the scaffolds make such structures susceptible to damage or collapse under storm conditions. This has led to a number of incidents reported over the past two decades, such as Uppark House, Surrey, which claimed two lives on 25th January 1990 (Maitra, 1994). Building damage is often caused by windblown scaffolding as well. The UK Health and Safety Executive (HSE, 1994) organized a conference into the wind loads on scaffold structures. Amongst the papers presented in this conference were those on wind damage (Blackmore, 1994), design of net clad structures (Williams, 1994) [2], full-scale tests (Hoxey, 1994) [3] and wind-tunnel tests (Schnabel, 1994).

Codes of practice such as those by the British Standards Institution, BS 5975 (BSI, 1996), and in European Codes BS EN 12810 (BSI, 2003), BS EN 12812 (BSI, 2004) include techniques for assessing the increase in tie loading due to wind. Despite this, there have been a number of incidents in recent years where scaffolding has fallen from buildings during storm conditions.

In the current design and analysis of scaffolds, the wind loads are derived from experiments conducted on permanent structures and limited allowance is made for the presence of the façades of the building to which the scaffold is attached. Limited research using CFD has been reported to determine the wind loads on temporary structures. Huang et al (2007) [4] used CFD to determine wind loads on high lift structures. Recently Amoroso et al (2010, 2011) [5,6] reported the results of wind tunnel tests on partially clad structures which complement the results reported in this paper and Giannoulis et al (2010) investigated, both experimentally in the field, and by CFD the airflow around a raised permeable panel which could be used to simulate the wind load on net cladded scaffolds. The authors have reported preliminary studies in (Irtaza et al, 2007) [7] and (Irtaza et al, 2009a,b) [8,9]. Due to the highly turbulent nature of the atmospheric boundary layer non-aerodynamic bluff bodies need a large computational domain for external flow fields.

Keeping this in mind a model scale of 1:30 of Silsoe Experimental Building (SEB) was selected as a base model and a scaffold cladded with net were considered for this study. The simulation was done on the basis of Silsoe Research Institute (SRI) full-scale data. The velocity profile and the longitudinal turbulence intensities simulated were obtained from SRI site (Richards et al, 2007) [10]. Three different unsteady CFD models, namely Renormalization (RNG) $k-\varepsilon$, Realizable $k-\varepsilon$ and Reynolds stress model are available in Fluent version 6.3 (Fluent, 2006) and were used to determine the pressure coefficients on the outer and inner face of the net clad scaffolds.

2. Simulation of Nets as Porous Media

A net can neither be tested as an aeroelastic model nor as a scaled model in a wind tunnel. This is because a thin net cannot be scaled further and also instrumentation is not available at the moment to be used for wind-tunnel modelling within nets.

The thin debris net was simplified in the porous media model as a "porous jump" with known velocity/pressure-drop characteristics and was applied to all the faces of the media. The porous jump model was applied to a face zone because it is more robust and yields good convergence. It incorporates an empirically determined flow resistance in a region of model defined as "porous" and is nothing more than an added momentum sink in the governing momentum equations. The Porous media were modelled by the addition of a momentum source term to the standard fluid flow equations. The source term is composed of two parts: a viscous loss term and an inertial loss term (Fluent, 2006).

$$S_i = -\left(\sum_{j=1}^{3} D_{ij} \mu v_j + \sum_{j=1}^{3} C_{ij} \frac{1}{2} \rho v_{mag} v_j \right) \tag{1}$$

where S_i is the source term for the i^{th} (x, y or z) momentum equation, and D and C are prescribed matrices. This momentum sink contributes to the pressure gradient in the porous cell, creating a pressure drop that is proportional to the fluid velocity (or velocity squared) in the cell (Fluent, 2006). To recover the case of a simple homogeneous porous media:

$$S_i = -\left(\frac{\mu}{\alpha} v_i + C_2 \frac{1}{2} \rho v_{mag} v_i \right) \tag{2}$$

where α is the permeability and C_2 is the inertial resistance factor, D and C are specified as diagonal matrices with $1/\alpha$ and C_2, respectively, on the diagonals (and zero for the other elements).

3. Wind-tunnel Tests on Nets

Two types of net (called Type A and Type B) were used here for the simulation as porous media and are shown in Fig. 2. In the wind-tunnel a section of each net was placed within a rectangular frame and inserted into the wind-tunnel completely filling the cross section of the tunnel. It was manufactured from high density polythene monofilaments. The Type B net was made by double folding the Type A net. The two nets were tested for drop in pressure versus velocity in the small wind-tunnel of the School of Technology, Oxford Brookes University of cross-section 305 mm × 305 mm. This is a non-boundary-layer wind-tunnel, of the open-circuit type, constructed mainly in aluminium and supported by a tubular steel framework.

These nets were tested in the wind-tunnel to determine the drop in pressures versus the velocity so as to simulate the nets as porous media and to determine the coefficients for the porous media. The mean thicknesses of the nets were measured with the help of digital micrometer screw gauge. Their average approximate thicknesses were measured to be 0.42 mm and 0.65 mm for Type A and B nets respectively. The experimental data obtained for the Net Type A and Type B have been plotted in Fig. 3 to create trend lines through the points yielding the following equations:

Type A net $$\Delta p = 0.524v^2 + 1.082v \tag{3}$$

Type B net $$\Delta p = 1.238v^2 + 2.249v \tag{4}$$

where Δp is the pressure drop and v is the velocity. Note that a simplified version of the momentum equation, relating the pressure drop to the source term, can be expressed as (Fluent, 2006):

$$\Delta p = -S \Delta n \tag{5}$$

where Δn is the thickness of the media giving the porous jump.

Hence, comparing Eq. (5) and Eq. (6) with $\Delta p = -\left(\frac{\mu}{\alpha} v + C_2 \frac{1}{2} \rho v^2 \right) \Delta n$ (from Eq. (4)) yields the following curve coefficients:

Type A net $$0.524 = C_2 \frac{1}{2} \rho \Delta n \tag{6}$$

Type B net $$1.238 = C_2 \frac{1}{2} \rho \Delta n \tag{7}$$

with $\rho = 1.225$ *kg/m*^{3}, and a porous media thickness Δn equal to 0.42 mm and 0.65 mm for Type A and Type B nets respectively. The inertial resistance factors are $C_2 = 2037\ 1/m$ for Type A and $C_2 = 3110\ 1/m$ for Type B respectively. Likewise,

Type A net $$1.082 = \frac{\mu}{\alpha}\Delta n \quad (8)$$

Type B net $$2.249 = \frac{\mu}{\alpha}\Delta n \quad (9)$$

With $\mu = 1.7894\times10^{-5}$, the viscous inertial resistance factor (1/permeability) $\alpha = 6.946\times10^{-9}\,m^2$ and $5.172\times10^{-9}\,m^2$ for Type A and Type B nets respectively.

4. Computational Solution Strategies

The cubical Silsoe Experimental Building was 6 m x 6 m x 6 m and the reduced scale used here for the simulation is 1:30. Scaffolds cladded with net were placed 1.50 m (prototype) from the facade of the building as shown in Fig. 7. The model of the net clad scaffold then simulated in Fluent. The Reynolds numbers involved in the simulations were in the range of 0.72×10^5 to 1.09×10^5 for both wind-tunnel experiments and computational analyses. The computational domain covers 29B (where B is the outer dimension of net clad scaffold) in the stream wise X direction $\left[-6.5 < (x/B) < 22.5\right]$, 13B in the lateral or normal (Z) direction $\left[-6.5 < (x/B) < 6.5\right]$ and 4H in the vertical (Y) direction. The percentage obstructions were 2.564 and 1.92 for the two cases described below which are less than the maximum 3% of obstruction required for good wind-tunnel models and for CFD simulation. The reason for the choice was to eliminate the flow obstacle effect on the inflow and outflow boundary conditions.

Fig. 4 shows the mesh arrangement for net clad scaffold model. For the net clad scaffold structured meshes were used as it was easier to generate. This arrangement made it easier to generate a mesh fine enough in the neighbourhood of the model whilst keeping the mesh in zones far away from the model surfaces unchanged or in a proper coarse state. An important advantage of this arrangement was that the mesh aligned to the model surfaces did not need to be stretched with the wall boundary layer grid as a structured mesh would have required.

5. Verification of Model

In order to validate the computational strategies used to determine the pressure coefficients a computational model of the Silsoe building was developed and the pressures found by the different numerical procedures compared against wind-tunnel model (Irtaza, 2009, Irtaza et al, 2010). The pressure coefficients at H/2 around the cube and over the cube at mid section are given in Figs. 5 and 6 where it can be seen that good agreement is obtained by all analyses along the sides and over the roof. The methods tend to overestimate the pressure coefficients on the windward face except for the LES procedure and underestimate the pressures on the leeward face. The wind-tunnel pressures are those recorded in (Irtaza et al 2010) which are in good agreement with pressures found from other investigators.

6. Results and Discussions

To determine the wind forces on net clad scaffolds the Silsoe building was used as a base model and a simulated scaffold erected around as shown in Fig. 7. The solid lines shown on the net clad scaffold models are the positions where the pressure coefficients measured while 0 to 1 is on the windward face, 1 to 2 on a side face and 2 to 3 on the leeward face of the net clad scaffold. The pressure coefficients were measured at two different heights i.e. at 0.5H and 2/3H from the ground respectively. . The pressure coefficients were also measured in the vertical direction in the middle of either width or depth of the scaffold (perpendicular to the ground) on both the inner and outer faces.

The simulated data from the wind-tunnel tests as explained above were used as input for different computational techniques used and a procedure was developed to extend the computational model to net clad scaffolds with the netting simulated as porous media. The netting properties such as its permeability and inertial resistance factor were obtained from wind-tunnel tests on nets as explained above.

The unsteady RNG $k-\varepsilon$, Realizable $k-\varepsilon$ and Reynolds stress methods (RSM) were used for computations over a period of 4 seconds. The time step was taken to be 0.001s and 4000 time steps performed. These were iterated to obtain the time averaged results for each time step. The porous jump boundary condition

was used for all nets in their respective directions. A turbulence intensity of 18% and a length scale of 0.3 at the eave height were kept constant for all the trials. The turbulence intensity was taken to match that of the Silsoe full-scale test.

The difference of pressure coefficients between outer and inner faces on all the façades of the net and for both type of nets is also plotted to determine the wind forces transferred from the net to the steel scaffold as shown in Figs 8 to 11 . The patterns of the pressure coefficients by all the three models on the windward outer and inner face were almost the same. However, on the side face the suction (negative) pressure coefficients shown by the RSM are the highest, followed by the Realizable $k-\varepsilon$ and the least by the RNG $k-\varepsilon$. Also on the leeward face the pressure coefficients shown by the RSM are higher than those found by the RNG and Realizable $k-\varepsilon$.

The drops in pressure coefficients are more for the Type B Net than for the Type A Net. This is because the Type B Net is denser than the Type A Net and therefore offers most resistance to flow. For Type B Net also the Reynolds stress model gives higher suction pressure than the RNG $k-\varepsilon$ and Realizable $k-\varepsilon$ models both on the side and leeward face. It was also observed that the Reynolds stress model showed a higher suction than the RNG $k-\varepsilon$ and the Realizable $k-\varepsilon$ model on the leeward side of the net.

The net clad scaffolds around the Silsoe Experimental Building were divided into different zones as seen in Fig. 12. The difference of pressure coefficients between inside and outside faces over different zones around the scaffolds for both types of net clad was determined and integrated numerically over the zones to calculate the average pressure for two types of net used. The resulting zone pressures are shown in Tables 2 to 5.

The flow patterns predicted by the RNG $k-\varepsilon$ model are shown in Figs. 13. The differences from other model plots are small. The flow features suggested by Wright and Easom (2003) were captured by the authors' numerical simulations, in particular the location and shape of the arch vortex in the wake. The turbulence is excessively over predicted by the Reynolds stress method on the side wall face and leeward face, an unrealizable turbulent kinetic energy is seen near the sharp end. The over-production of turbulent viscosity results in the prediction of small separation bubbles and a large downstream arch vortex.

To see if these results were fully representative, a two-dimensional parametric study of the building in plan was undertaken with nets having permeabilities varying from $1.0\times10^{-6}\,\mathrm{m}^2$ to $1.0\times10^{-10}\,\mathrm{m}^2$ and having the inertial constant C_2 (inertial resistance constant) equal to zero were also simulated with all other data kept the same as that used for the Type A and Type B nets. A permeability of $1.0\times10^{-10}\,\mathrm{m}^2$ corresponds to a nearly impermeable sheet and a permeability of $1.0\times10^{-6}\,\mathrm{m}^2$ corresponds to a very permeable sheet (almost non-existing). The resulting pressure coefficients are shown in Fig. 14. The pressure distribution for the net with permeability $1.0\times10^{-10}\,\mathrm{m}^2$ corresponds to that found by the authors when analysing a completely impermeable sheet (Irtaza et al 2009a). Similarly the pressure distribution for the very permeable net, $1.0\times10^{-10}\,\mathrm{m}^2$, corresponded to the distribution around an unsheeted building. The CFD analyses for a building surrounded by an impermeable sheet and around a building with no scaffolding attached had good agreement with a wind-tunnel experiments; hence showing that in the limits the permeable CFD model was able to agree with both extremes, giving confidence in its ability to predict pressure distributions. The mean value of the pressure difference on the impermeable sheeting on the windward face of the building is 1.46, slightly higher than the 1.3 used in the German code of practice (DIN, 2004).

7. Conclusions

The behaviour of fabric clad (net/sheet) on scaffold structures in a wind is extremely complex and aeroelastic in nature. The wind forces acting on scaffolds (transferring from covering materials to the scaffold support structure) depends mainly on the air penetrability of the netting and of the building. The permeabilities of the nets were calculated from the graphs plotted between free stream velocity versus drop in pressure across the net (from wind-tunnel experiments) by assuming that the drop in pressure across the nets is proportional to the inertial resistance and inversely proportional to the permeability.

The difference in the pressure coefficients between the outer and the inner faces on all the façades of the net and for both type of nets (Type A Net and Type B Net) were plotted to determine the wind forces transferred from the net to the supporting scaffold. The nets were simulated as porous media. The pattern of the pressure coefficients by all the three CFD models on the windward outer and inner faces were almost the same. However, on the side face the suction (negative) pressure coefficients shown by RSM are the highest, followed by the Realizable $k-\varepsilon$ and the least by the RNG $k-\varepsilon$ models. On the leeward face the pressure coefficients shown by RSM are higher than those found by the RNG and Realizable $k-\varepsilon$.

The different zones on net clad scaffolds for taking pressure coefficient values are shown in Fig. 16 and taking the mean values of the results in Tables 2 to 5 recommended zone values are given in Table 6. From this table it can be seen that there is no need to consider wind forces on the leeward face of the net clad or elevated net clad scaffold as there is suction of nearly equal magnitude on both sides of the leeward net which cancels the forces.

The parametric study showed that the results for net clad scaffold were validated against the extremes of a fully clad scaffold and a building without scaffolding.

References

[1] Beale R.G. (2007), "Review of Research into Scaffold Structures". Civil Engineering Computations: Tools and Techniques, Saxe-Coburg Publications, Ch 12, 271-300.
[2] Williams, C.J.K. (1994), "The structural design of fabric structures to resist wind loading", Proceedings of the Conference into Wind Loading on Temporary Structures, Buxton, HSE, UK.
[3] Hoxey, R. (1994), "Full-scale studies of wind-loading on light-weight structures, windbreaks and walls at Silsoe Research Institute", Proceedings of the Conference into Wind Loading on Temporary Structures, Buxton, HSE, UK.
[4] Huang, S., Li, Q.S. and Xu, S. (2007), "Numerical evaluation of wind effects on a tall steel building by CFD", J. Const. Steel Res., **63**(4), 448-459.
[5] Amoroso, S., Hebert, K. and Levitan, M., (2010), "Wind tunnel tests for mean wind loads on partially clad structures". J. Wind Eng. Ind. Aerod., **98**(12), 689-700.
[6] Amoroso, S.D. and Levitan, M.L. (2011), "Wind loads for high-solidity open-frame structures", J. Wind. Struct., **14**(1), 1-14.
[7] Blackmore, P.A. (1994), "The history of wind damage in the UK", Proceedings of the Conference into Wind Loading on Temporary Structures, Buxton, HSE, UK.
[8] Irtaza, H., Beale, R.G., Godley, M.H.R. 'Determination of the effects of the wind load on bare tube access scaffold structures using Computational Fluid Dynamics', 5th International Conference on Advances in Steel Structures (ICASS 2007), Singapore, December 5-7, 2007.
[9] Irtaza, H., Beale, R.G. and Godley, M.H.R. (2009a), "Experimental and Numerical Evaluation of Computational Fluid Dynamics of Wind Loads on Sheeted Scaffolds", Proceedings 12th International Conference on Civil, Structural and Environmental Engineering Computing, Funchal, Paper 261, 19p.
[10] Irtaza, H., Beale, R.G. and Godley, M.H.R. (2009b), "Wind Loads on Netted Metal Access Scaffolds", Proceedings of the 6th International Conference on Advances in Steel Structures (ICASS'09), Hong Kong, 1091-1098.
[11] Richards, P.J., Hoxey, R.P. Connell, B.D. and Lander, D.P. (2007), "Wind-tunnel modelling of Silsoe Cube", J. Wind Eng. Ind. Aerod., **95**(9-11), 1384-1399.

Table 1. Average pressure coefficient differences on net clad scaffolds for Type A Net at Z=0.5H

Net Clad Scaffold Surrounding the SEB (touching the ground)
Net Type A, Z = 0.5H

CFD	Windward Face			Side Face		Leeward Face
Technique	Zone A	Zone B	Zone C	Zone D	Zone E	Zone F
RNGKE	0.273	0.166	0.273	-0.108	0.003	-0.0235
RKE	0.288	0.1605	0.288	-0.063	-0.002	-0.0438
RSM	0.278	0.163	0.278	-0.102	0.003	-0.0238

Table 2. Average pressure coefficient differences on net clad scaffolds for Type B Net at Z=0.5H

Net Clad Scaffold Surrounding the SEB (touching the ground)
Net Type B, Z = 0.5H

CFD	Windward Face			Side Face		Leeward Face
Technique	Zone A	Zone B	Zone C	Zone D	Zone E	Zone F
RNGKE	0.431	0.343	0.431	-0.193	-0.007	-0.0441
RKE	0.429	0.318	0.429	-0.131	-0.012	-0.0665
RSM	0.425	0.331	0.425	-0.177	-0.001	-0.0380

Table 3. Average pressure coefficient differences on net clad scaffolds for Type A Net at Z=2/3H

Net Clad Scaffold Surrounding the SEB (touching the ground)
Net Type A, Z = 2/3H

CFD	Windward Face			Side Face		Leeward Face
Technique	Zone A	Zone B	Zone C	Zone D	Zone E	Zone F
RNGKE	0.307	0.196	0.307	-0.088	0.0072	-0.042
RKE	0.322	0.188	0.322	-0.037	-0.0007	-0.063

RSM	0.310	0.192	0.310	-0.074	0.0064	-0.044

Table 4 Average pressure coefficient differences on net clad scaffolds for Type B Net at Z=2/3H

Net Clad Scaffold Surrounding the SEB (touching the ground)						
Net Type B, Z = 2/3H						
CFD Technique	Windward Face			Side Face		Leeward Face
	Zone A	Zone B	Zone C	Zone D	Zone E	Zone F
RNGKE	0.461	0.367	0.461	-0.1622	-0.0037	-0.0615
RKE	0.449	0.333	0.449	-0.0972	-0.0109	-0.0874
RSM	0.447	0.350	0.447	-0.1392	-0.0003	-0.0522

Table 6. Recommended pressure coefficients on net/elevated net clad scaffolds

Net Clad Scaffold Surrounding the SEB (touching the ground)						
Design Pressure Coefficients	Windward Face			Side Face		Leeward Face
	Zone A	Zone B	Zone C	Zone D	Zone E	Zone F
	0.37	0.26	0.37	- 0.11 (outward)	-	-

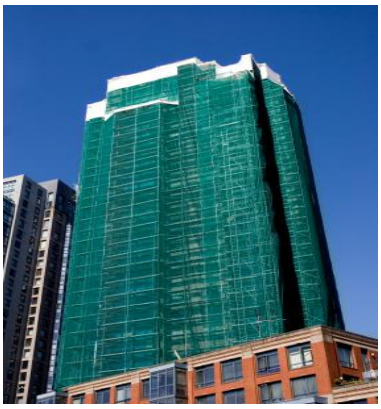

Fig. 1 Typical scaffolds surrounded by net

(a) Type A net

(b) Type B net

Fig. 2 Nets tested in wind-tunnel

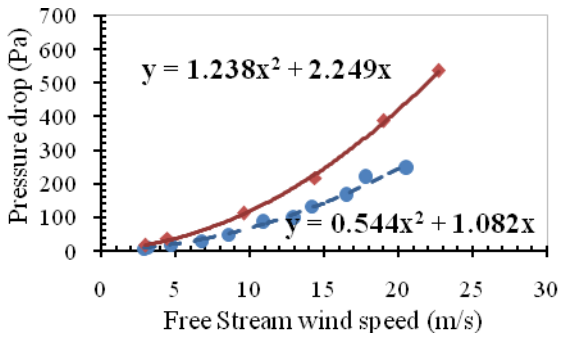

Fig. 3 Free stream wind speed versus pressure drop across the nets

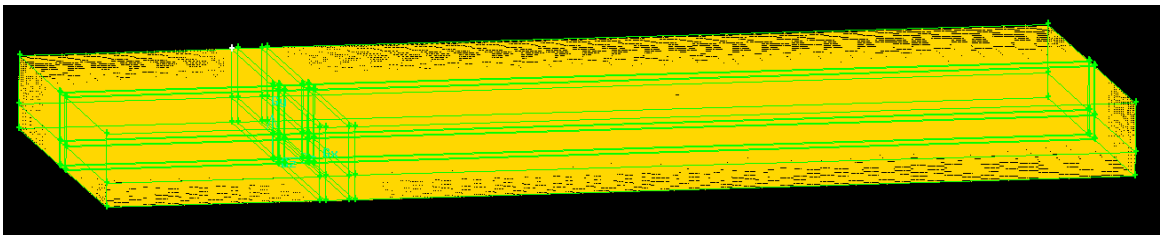

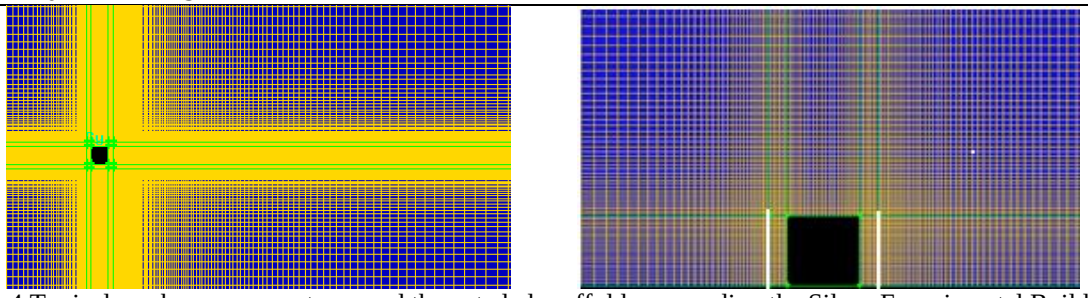

Fig. 4 Typical mesh arrangements around the net clad scaffold surrounding the Silsoe Experimental Building

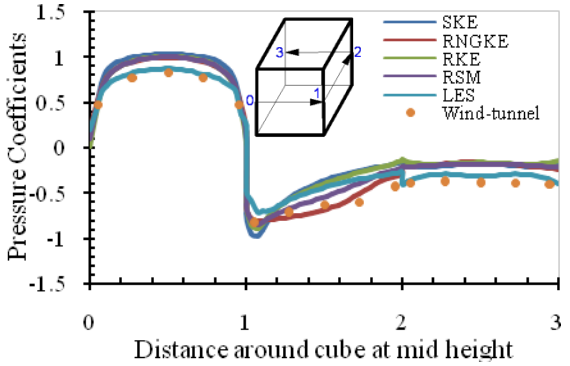

Fig 5 Comparison of mean pressures around the cube

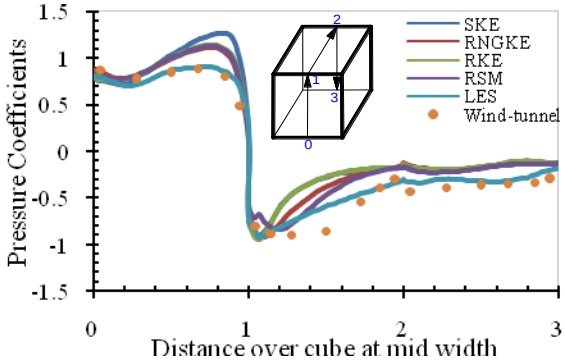

Fig 6 Comparison of mean pressures over the cube

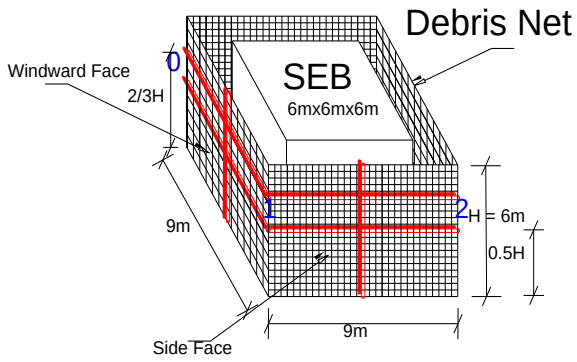

(a) Windward and side faces

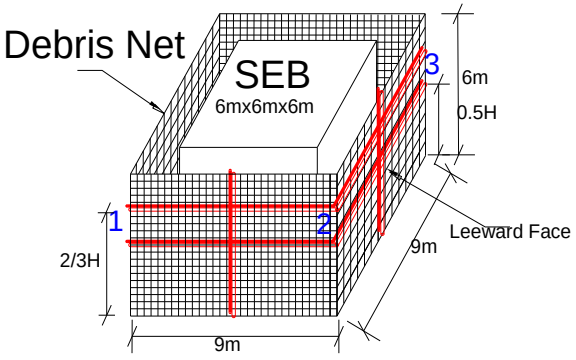

(b) Side and leeward faces

Fig. 7 Isometric views of the net clad scaffold surrounding the Silsoe Experimental Building

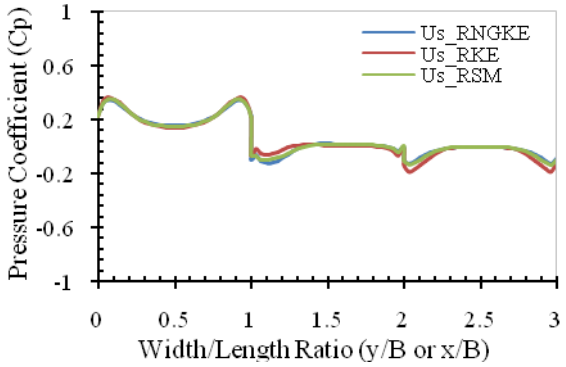

Fig. 8 Difference of Pressure Coefficients at two-thirds height for Type A Net

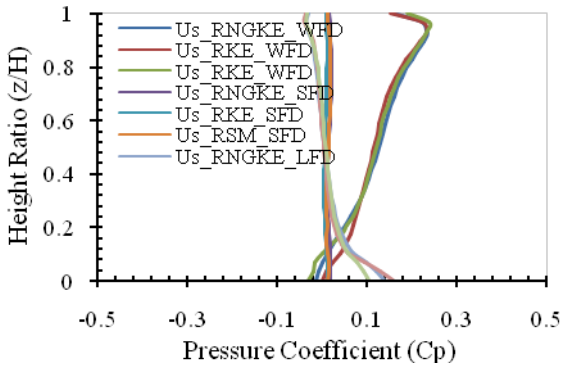

(c) Difference of pressures

Fig. 9 Difference of Pressure Coefficients around the scaffold at mid-width for Type A Net

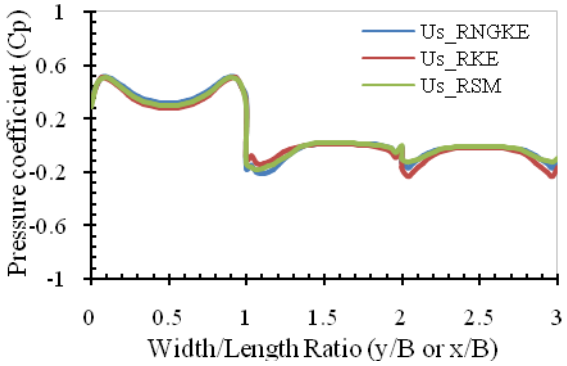

Fig. 10 Difference of Pressure Coefficients at two-thirds height for Type B Net

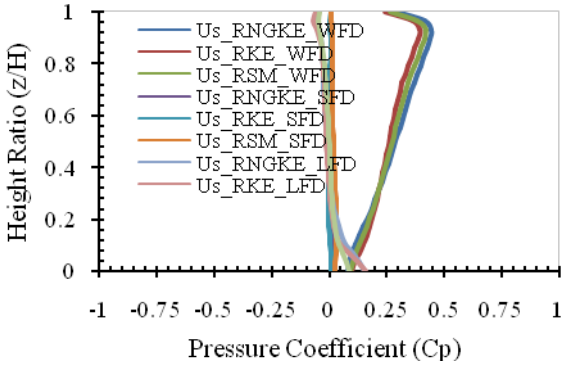

Fig. 11 Difference of Pressure coefficients around the net clad scaffold at mid-width for Type B Net

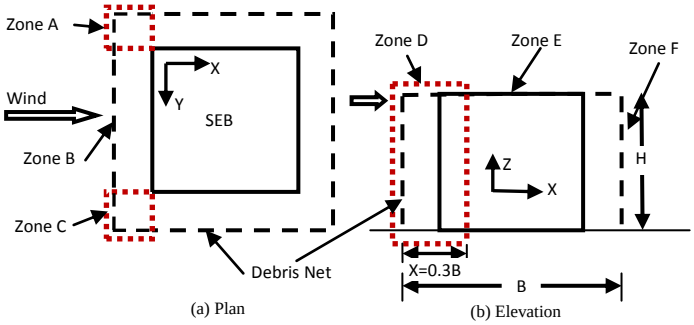

(a) Plan (b) Elevation

Fig. 12 Net clad scaffolds touching the ground surrounding the Silsoe Experimental Building

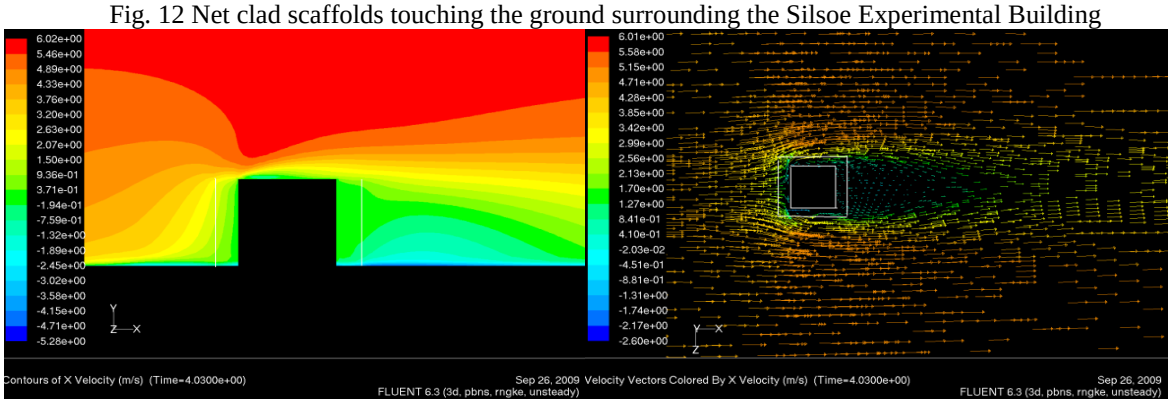

(a) X- velocity contours in section (b) Velocity vectors in plan

Fig. 13 Velocity contours and vectors, and turbulent energy contours for Type A Net, RNG $k-\varepsilon$ model

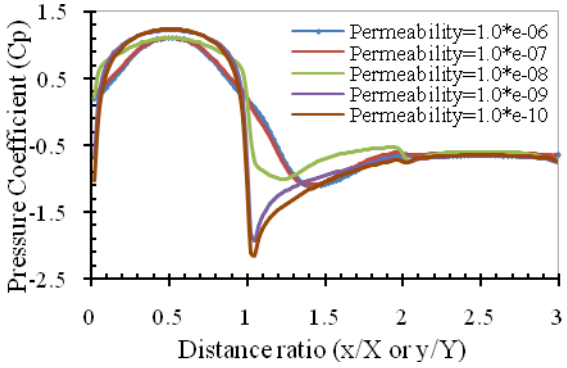

(a) Outer face

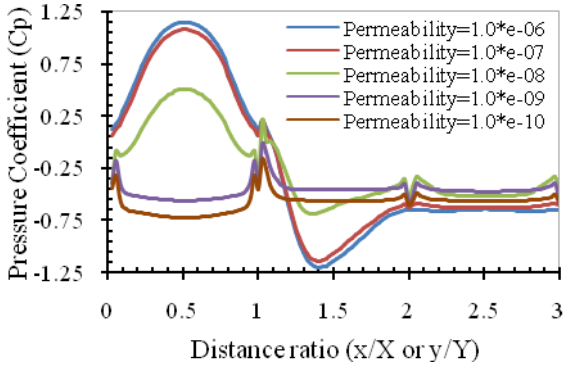

(b) Inner face

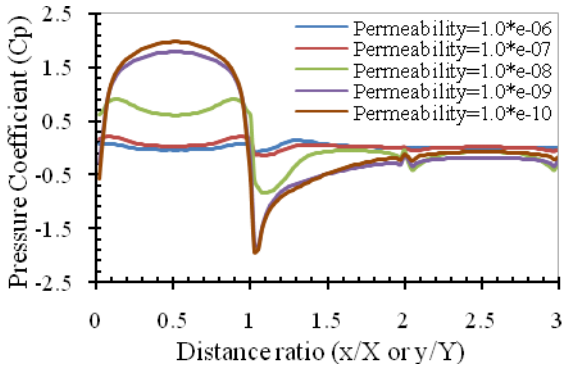

(c) Difference of pressure

Fig. 14 Parametric study of pressures around net clad scaffolds